Fiberlike Fe_2O_3 Macroporous Nanomaterials Fabricated by Calcinating Regenerate Cellulose Composite Fibers

Shilin Liu,[†] Lina Zhang,*[,†] Jinping Zhou,[†] Jiangfeng Xiang,[†] Jutang Sun,[†] and Jianguo Guan[‡]

Department of Chemistry, Wuhan University, Wuhan 430072, China, and State Key Laboratory of Advanced Technology for Materials Synthesis and Processing, Wuhan University of Technology, Wuhan 430070, China

Received December 19, 2007. Revised Manuscript Received March 31, 2008

Fiberlike Fe_2O_3 macroporous nanomaterials have been prepared by in situ synthesis of Fe_2O_3 nanoparticles in the regenerated cellulose fibers during the wet spinning process, followed by the removal of cellulose matrix by calcination. The interpenetrated porous structure in the regenerated cellulose fibers at swollen state could serve as templates for the preparation of inorganic nanoparticles. The structure and properties of the Fe_2O_3 nanomaterials were characterized with X-ray diffraction, scanning electron microscopy, magnetometer, and electrochemical tests. The Fe_2O_3 nanomaterials exhibited integrated one-dimensional (1D) fiberlike morphology with macroporous structure. The results revealed that the inorganic nanomaterials displayed high purity of α-Fe_2O_3 and possessed large specific surface area, weak ferromagnetic properties, and superior electrochemical activity, having a discharge capacity of 2750 mA·h/g. Due to the small amounts of waste generated, this work provided a "green" pathway for the preparation of 1D inorganic nanomaterials with retention of the macropore structure, which have potential applications in the functional material fields.

Introduction

Considerable attention has been focused on one-dimensional (1D) nanostructured materials due to their unique physical properties and potential applications.[1–3] Metal oxide nanoparticles are particularly attractive as building blocks for nanomaterial architectures. Compared to conventional bulk materials, low-dimensional nanoscale materials (with their large surface areas and possible quantum-confinement effects) exhibit improved and/or distinct electronic, [4] optical,[5] and magnetic properties[6] and catalytic power[7] etc., becoming potential candidates for many applications that could open new avenues of development in many areas. Much effort has been devoted to the synthesis of metal oxide nanomaterials with predefined geometries, such as two-dimensional (2D) and three-dimensional (3D) superstructures by self-assembly,[8–10] the Langmuir−Blodgett method,[11] or electrophoresis deposition.[12–14] Their optical and electron transport properties have also been investigated. It is noted that the potential applications of 1D arrays of nanomaterials in nanoelectronics, catalysts, magnetic storage media, sensors, and optical and micromechanical devices have increased emphasis in the area of nanotechnology and nanoscience.[15,16]

Hematite (α-Fe_2O_3) is the most stable iron oxide with n-type semiconducting properties under ambient conditions. Due to its low cost and high resistance to corrosion, it has been extensively used as catalysts,[17] gas sensors,[18] photoelectrodes for solar energy conversion,[19] clinical therapy and diagnosis,[20] etc. Stimulated by the intriguing properties and unique applications of the Fe_2O_3 materials at nanoscale, special attention has been given to these 1D nanostructures (nanowire and nanorod) by using methods such as hydrothermal synthesis,[21] chemical vapor deposition,[22] etc. In particular, increasing attention has been paid to ferromagnetic

* Corresponding author. Tel.: +86-27-87219274. Fax: +86-27-68754067. E-mail: lnzhang@public.wh.hb.cn.
[†] Wuhan University.
[‡] Wuhan University of Technology.

(1) Son, S. J.; Reihel, J.; He, B.; Schuchman, M.; Lee, S. B. *J. Am. Chem. Soc.* **2005**, *127*, 7136.
(2) Jia, C-J.; Sun, L-D.; Yan, Z-G.; You, L-P.; Luo, F.; Han, X-D.; Pang, Y-C.; Zhang, Z.; Yan, C-H. *Angew. Chem., Int. Ed.* **2005**, *44*, 4328.
(3) Sui, Y. C.; Skomski, R.; Sorge, K. D.; Sellmyer, D. J. *Appl. Phys. Lett.* **2004**, *84*, 1525.
(4) Becerril, H. A.; Stoltenberg, R. M.; Wheeler, D. R.; Davis, R. C.; Harb, J. N.; Woolley, A. *J. Am. Chem. Soc.* **2005**, *127*, 2828.
(5) Chae, W.-S.; Lee, S.-W.; Im, S.-J.; Moon, S.-W.; Zin, W.-C.; Lee, J.-K.; Kim, Y.-R. *Chem. Commun.* **2004**, 2554.
(6) Zhou, P.; Xue, D.; Luo, H.; Chen, X. *Nano. Lett.* **2002**, *2*, 845.
(7) Zhan, S.; Chen, D.; Jiao, X.; Song, Y. *Chem. Commun.* **2007**, 2043.
(8) De, G.; Köhn, R.; Xomeritakis, G.; Brinker, C. J. *Chem. Commun.* **2007**, 1840.
(9) Howorka, S. *J. Mater. Chem.* **2007**, *17*, 2049.
(10) Lu, N.; Chen, X.; Molenda, D.; Naber, A.; Fuchs, H.; Talapin, D. V.; Weller, H.; Mller, J.; Lupton, J. M.; Feldmann, J.; Rogach, A.; Chi, L. *Nano. Lett* **2004**, *4*, 885.
(11) Kim, F.; Kwan, J.; Akana, J.; Yang, P. *J. Am. Chem. Soc.* **2001**, *123*, 4360.
(12) Bertoncello, P.; Peruffo, M.; Unwin, P. R. *Chem. Commun.* **2007**, 1597.
(13) Cong, H.; Cao, W. *Adv. Funct. Mater.* **2005**, *15*, 1821.
(14) Li, Q.; Newberg, J. T.; Walter, E. C.; Hemminer, J. C.; Penner, R. M. *Nano Lett.* **2004**, *4*, 277.
(15) Patel, A. C.; Li, S.; Wang, C.; Zhang, W.; Wei, Y. *Chem. Mater.* **2007**, *19*, 1231.
(16) Lu, X.; Zhang, D.; Zhao, Q.; Wang, C.; Zhang, W.; Wei, Y. *Macromol. Rapid Commun.* **2006**, *27*, 76.
(17) Liu, Q.; Cui, Z.-M.; Ma, Z.; Bian, S.-W.; Song, W.-G.; Wan, L.-J. *Nanotechnology* **2007**, *18*, 384605.
(18) Chen, J.; Xu, L.; Li, W.; Gou, X. *Adv. Mater.* **2005**, *17*, 582.
(19) Ohmori, T.; Takahashi, H.; Mametsuka, H.; Suzuki, E. *Phys. Chem. Chem. Phys.* **2000**, *2*, 3519.
(20) Zhang, Y.; Kohler, N.; Zhang, M. *Biomaterials* **2002**, *23*, 1553.

10.1021/cm703623v CCC: $40.75
Published on Web 05/10/2008

nanomaterials, microsized nanowalls, and nano-/micropatterns of magnetic iron oxides, the macroporous monoliths of functional inorganic materials through template-free routes.[23,24] However, facile and low-cost as well as "green" physicochemical methods for the preparation of the 1D nanomaterials have been scarcely reported.

In our laboratory, a novel solvent of 7.0 wt % NaOH/12.0 wt % urea aqueous solutions precooled to −12 °C has been developed to dissolve cellulose.[25] Moreover, regenerated cellulose films and fibers with good structure and properties have been prepared successfully from the cellulose dope.[26–30] It is worth noting that the cellulose fibers or films in the wet state exhibit porous structure, which can be controlled by changing coagulant, polymer concentration, temperature, etc. Furthermore, the preparation of cellulose materials is a "green" process. We are interested in the preparation of 1D inorganic nanomaterials on the basis of the porous structure of regenerated cellulose fibers in the wet state. In this work, we try to develop a simple method for the preparation of a fiberlike Fe_2O_3 porous material by calcination of regenerated cellulose fibers containing individual Fe_2O_3nanoparticles, which can be synthesized in situ. The structure and properties of the porous fiberlike Fe_2O_3 were characterized with X-ray diffraction, scanning electron microscopy, magnetometer, and electrochemical testing. We provided here a new conceptual scheme for the design and fabrication of 1D inorganic material, hoping to open up new application areas for cellulose fibers as well as for the fabricated inorganic nanomaterials.

Experimental Section

Materials. The cellulose sample (cotton linter pulp, α-cellulose >95%) was provided by Hubei Chemical Fiber Group Ltd. (Xiangfan, China). Its viscosity-average molecular weight (M_η) was determined by using an Ubbelohde viscometer in LiOH/urea aqueous solution at 25 ± 0.05 °C and calculated from the equation[31] $[\eta] = 3.72 \times 10^{-2} M_w^{0.77}$ to be 8.1×10^4. Other analytical-grade chemical regents were purchased in China and used without further purification.

Preparation of Fiberlike Fe_2O_3. A solution with NaOH/urea/H_2O ratio of 7:12:81 by weight was precooled to −12 °C. Then, cellulose with a desired amount was immediately dispersed into the solvent system (3 L) under vigorous stirring for 15 min at ambient temperature below 20 °C to obtain a transparent cellulose dope with a concentration of 4.8 wt %. The fibers were made by wet spinning on a pilot spinning machine manufactured by Hubei Chemical Fiber Group Ltd. according to our report.[29] The spinneret cylinder was immersed directly into the first coagulation bath containing 9.9 wt % H_2SO_4/10 wt % Na_2SO_4 at 19 °C by wet spinning. The gelation fibers solidified in the first coagulation bath were taken up on the first roller and then drawn to the second roller. Subsequently, the fibers were drawn from the second roller into the second coagulation bath containing 5 wt % H_2SO_4. The fibers, after washing by running water, were drawn into a container with different concentrations of $FeCl_3$ aqueous solution and kept for various periods of time. They were then removed to another container containing 2 M NaOH solution and treated for 20 min to obtain cellulose/Fe_2O_3 composite fibers. These treated fibers were washed with deionized water and then rolled up and dried at ambient temperature. The cellulose fiber sample that was not treated with $FeCl_3$ solution was coded as regenerated cellulose fibers (RC). The cellulose fibers treated with $FeCl_3$ solution with a concentration of 0.01, 0.1, and 0.5 M were coded as F001, F01, and F05, respectively. The cellulose fibers treated with the same $FeCl_3$ solution for 10, 30, 120, and 300 min were coded as F0510, F0530, F05120, and F05300, respectively. The F001, F01, and F05 composite fibers were sintered at 600 ± 5 °C under an air atmosphere for 3 h in a muffle to obtain fiberlike Fe_2O_3 materials, coded as FE001, FE01, and FE05, respectively.

Characterization. Wide-angle X-ray diffraction (XRD) measurement was carried out on a XRD diffractometer (D8-Advance, Bruker, U.S.). The patterns with Cu Kα radiation ($\lambda = 0.15406$ nm) at 40 kV and 30 mA were recorded in the region of 2θ from 5 to 70°. Samples were ground into powders and dried in a vacuum oven at 60 °C for 48 h. Transmission electron microscopy (TEM) images were obtained on a JEOL JEM-2010 (HT) electron microscope, using an accelerating voltage of 200 kV. Scanning electron microscopy (SEM) measurements were carried out on a FESEM (SEM, SIRION TMP, FEI) by using an accelerating voltage of 20 kV; the samples were coated with gold to facilitate SEM observation. Nitrogen adsorption−desorption measurements were performed by using an ASAP 2020 (Micromeritics, U.S.) volumetric adsorption apparatus. Thermal gravimetric analysis (TGA) was carried out with a thermogravimetric analyzer (Netzsch, German). The fibers were ground into powder and about 5 mg of the powder was placed in a platinum pan and heated from 20 to 600 °C at a rate of 10 k/min in an air atmosphere.

The magnetic property measurement of the Fe_2O_3 fibers was carried out on a vibrating sample magnetometer (VSM, model 4HF, ADE Ltd. Co., U.S.), and the magnetic field reached up to 1.7 T. The charge/discharge tests were carried out using the coin-type cell (size: 2016) at 20 °C, which consisted of a Fe_2O_3 working electrode and a lithium foil counter separated by a Celgard 2004 microporous membrane. The electrode was prepared by mixing Fe_2O_3 samples with 15% acetylene black and 5% polytetrafluoroethylene (PTFE) binder and compressing the mixture onto an aluminum mesh current collector. $LiPF_6$ (1 M) dissolved in ethylene carbonate/dimethyl carbonate (EC/DMC, 1:1 volume ratio) was used as the electrolyte. The electrochemical tests were examined on a Neware cell test system. The cells were assembled in an argon-filled glovebox (Mikrouna, Super 1200/750, China) and were charged and discharged at a constant current density of 100 mA/g.

Results and Discussion

The nanocomposite fibers containing Fe_2O_3 nanoparticles have been fabricated successfully via wet spinning from the cellulose dope in aqueous NaOH/urea solution by in situ synthesis. The morphology and structure of the RC fibers and the composite fibers are shown in Figure 1. The RC fibers have a round cross section with diameter of about 45

(21) Zhong, Z.; Ho, J.; Teo, J.; Shen, S.; Gedanken, A. *Chem. Mater.* **2007**, *19*, 4776.
(22) Wu, J.-J.; Lee, Y.-L.; Chiang, H.-H.; Wong, D. K.-P. *J. Phys. Chem. B* **2006**, *110*, 18108.
(23) Zong, B.; Wu, Y.; Han, G.; Yang, B.; Luo, P.; Wang, L.; Qiu, J.; Li, K. *Chem. Mater.* **2005**, *17*, 1515.
(24) Toberer, E. S.; Joshi, A.; Seshadri, R. *Chem. Mater.* **2005**, *17*, 2142.
(25) Cai, J.; Zhang, L. *Macromol. Biosci.* **2005**, *5*, 539.
(26) Mao, Y.; Zhou, J.; Cai, J.; Zhang, L. *J. Membr. Sci.* **2006**, *279*, 246.
(27) Zhang, L.; Mao, Y.; Zhou, J.; Cai, J. *Ind. Eng. Chem. Res.* **2005**, *44*, 522.
(28) Cai, J.; Zhang, L.; Zhou, J.; Li, H.; Chen, H.; Jin, H. *Macromol. Rapid Commun.* **2004**, *25*, 558.
(29) Cai, J.; Zhang, L.; Zhou, J.; Qi, H.; Chen, H.; Kondo, T.; Chen, X.; Chu, B. *Adv. Mater.* **2007**, *19*, 821.
(30) Cai, J.; Zhang, L. *Cellulose* **2007**, *14*, 205.
(31) Cai, J.; Liu, Y.; Zhang, L. *J. Polym. Sci., Part B: Polym. Phys.* **2006**, *44*, 3093.

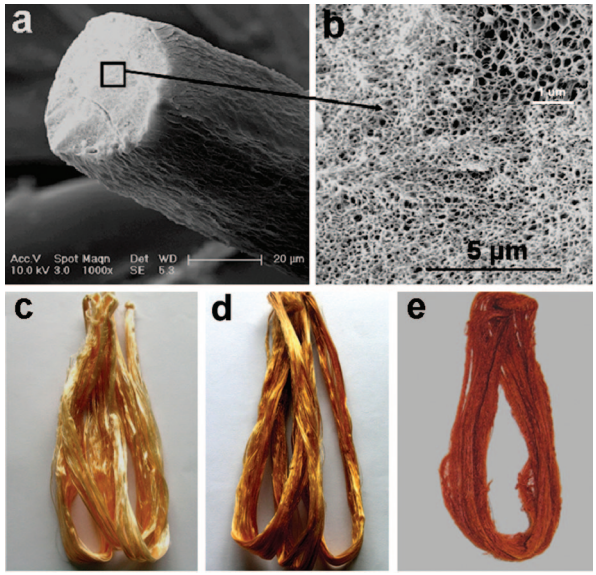

Figure 1. SEM images of surface (a) and cross section (b) for a single swollen RC fiber (insert is its enlarged image and the scale bar is 1 μm), as well as photographs of the composite fibers F001 (c), F01 (d), and F05 (e), respectively.

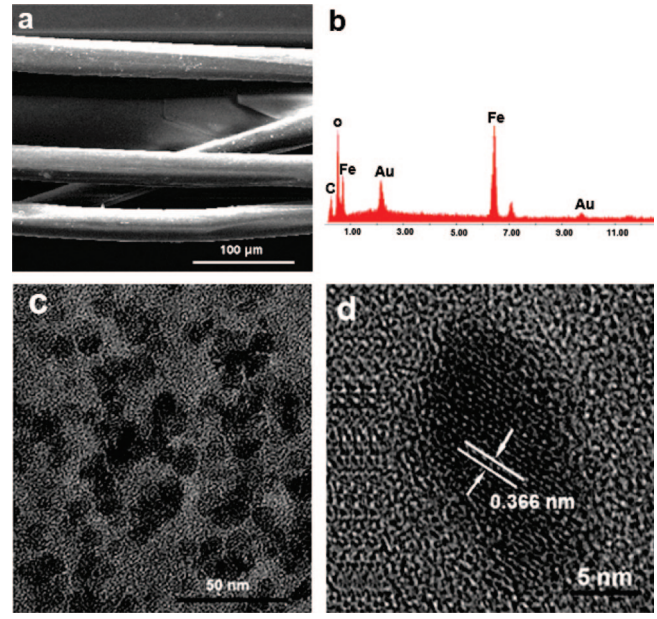

Figure 2. SEM (a) and TEM (c, d) images of the Fe_2O_3/cellulose composite fibers (F05), as well as the EDS spectrum (b) from SEM, (d) HRTEM pattern of (c).

μm in the swollen state (Figure 1a), and their interior exhibits macroporous mesh structure with a mean pore diameter of about 150 nm (Figure 1b). The structure was observed from the freeze-dried state of the swollen regenerated cellulose fibers. Therefore, it is plausible that the regenerated cellulose fibers in the swollen state have through-penetrated macroporous structure, which could serve as templates in which inorganic nanoparticles can be prepared homogeneously. Figures 1c−e show the photographs of the composite fibers treated with different concentrations of $FeCl_3$ solution and followed with 2 M NaOH solution. It is clearly shown that the colorless RC fibers changed from shallow yellow to brown with an increase of the concentration of $FeCl_3$ solution from 0.01 to 0.5 M. The colored fibers may be resulting from Plasmon absorption of the Fe_2O_3 component. It is worth noting that a strong interaction exists between the Fe_2O_3 component and the cellulose matrix because the detected mass of the Fe_2O_3 component removed from the composite fibers was negligible (15 μg/L) after immersing the fibers in water for 72 h (composite fibers/water = 1 wt %). The XRD and X-ray photoelectron spectroscopic (XPS) results have indicated that the crystalline phase of the Fe_2O_3 component in the composite fibers is ($\alpha + \gamma$) Fe_2O_3.[32]

The SEM and TEM images for the composite fibers (F05) are shown in Figure 2. The surface of the composite fibers (Figure 2a) is denser than that of RC fibers (see Figure S1 in the Supporting Information), and the diameter of the composite fibers in the dry state is about 27 μm. A shrinkage of the composite fibers has occurred during the drying process, leading to the formation of a denser structure and an enhancement of the interaction between the cellulose matrix and the Fe_2O_3 nanoparticles. The energy dispersive spectrum (EDS) measured from the FESEM has indicated that there are only C, O, and Fe elements in the composite fibers (Figure 2b). It further supports that Fe_2O_3 nanoparticles have been synthesized in the cellulose fibers. The TEM results indicate that Fe_2O_3 nanoparticles having a mean diameter of 18 nm are uniformly dispersed in the cellulose matrix (Figure 2c). The high-resolution TEM (HRTEM) image (Figure 2d) shows that the Fe_2O_3 nanoparticles in the cellulose fibers have been well-crystallized, and the lattice plane distance of 0.366 nm is in good agreement with the separation between the (012) lattice plane of α-Fe_2O_3 (Powder Diffraction file, JCPDS card no. 89-2810). The results have confirmed that the Fe_2O_3 nanoparticles have been synthesized successfully in situ in the regenerated cellulose fibers in the wet state.

The thermal stability of the RC fibers and composite fibers is shown in Figure 3. It is clear that the thermal stability properties of the cellulose fibers decrease with the loading of Fe_2O_3 nanoparticles. The cellulose fibers begin to decompose at ca. 353 °C, whereas in the case of the F05 fibers, the onset of the decomposition temperature is about 326 °C, which is 27 °C lower than that of the cellulose fibers. It is a result of the catalytic property of the Fe_2O_3 nanoparticles.[33,34] Interestingly, the content of Fe_2O_3 nanoparticles in the cellulose fibers increases rapidly from 0.17 to 11.08 wt % when the concentration of $FeCl_3$ changes from 0.01 to 0.5 M. The content of Fe_2O_3 nanoparticles in F05 is about 70 times that of F001, whereas the $FeCl_3$ concentration increases by 50 times. This difference in the content of the incorporated Fe_2O_3 nanoparticles may be ascribed to the diffusion equilibrium of Fe^{3+} between solution and the cellulose matrix.[35] Figure 3b shows the dependence of the content of Fe_2O_3 nanoparticles in F05 composite fibers on the immersion time in the $FeCl_3$ solution (0.5 M). The effect of the immersion

(32) Liu, S.; Zhang, L.; Zhou, J.; Wu, R. *J. Phys. Chem. C* **2008**, *112*, 4538.
(33) Ma, Z.; Li, F.; Bai, H. *Propellants, Explos., Pyrotech.* **2006**, *31*, 447.
(34) Shekhah, O.; Ranke, W.; Schule, A.; Kolios, G.; Schlogl, R. *Angew. Chem., Int. Ed.* **2003**, *42*, 5760.
(35) Kongdee, A.; Bechtold, T. *Dyes Pigm.* **2004**, *60*, 137.

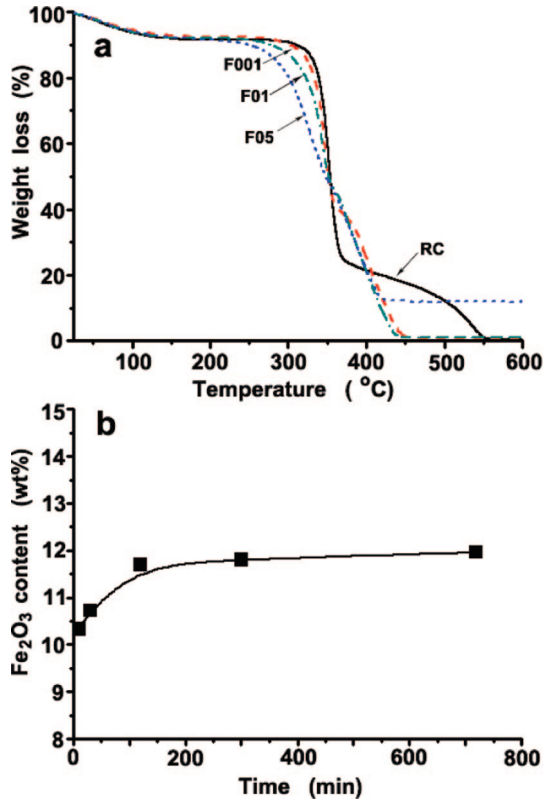

Figure 3. Weight loss (in percentage of the initial weight) as a function of temperature for the RC fibers and composite fibers (a), and the influence of the storage time for cellulose fibers immersed into $FeCl_3$ solution (0.5 M) on the content of the incorporated Fe_2O_3 nanoparticles (wt %) in the F05 composite fibers (b).

time on the Fe_2O_3 content in the composite cellulose fibers is not significant, suggesting that the diffusion equilibrium of Fe^{3+} between the cellulose matrix and the $FeCl_3$ solution has been reached rapidly. This result indicates that the concentration of $FeCl_3$ solution plays an important role in controlling the content of the Fe_2O_3 nanoparticles in the cellulose fibers. Within a relatively short treating time, the high content of Fe_2O_3 nanoparticles in cellulose fibers could be obtained via the increase of the $FeCl_3$ concentration.

Interestingly, after the complete removal of the cellulose matrix by calcination at 600 °C under an air atmosphere, the resulting Fe_2O_3 samples exhibit different structures and morphologies. Figure 4 shows the SEM images of the Fe_2O_3 samples (FE001, FE01, and FE05) after the removal of the cellulose matrix by calcination. When the $FeCl_3$ concentration was 0.01 M, the FE001 sample was uniform without the fiberlike morphology as shown in Figure 4a. However, when the $FeCl_3$ concentration was 0.1 and 0.5 M, respectively, the FE01 sample exhibited a fiberlike morphology with a faulty structure as shown in Figure 4b, and the FE05 sample displayed an integrated 1D fiberlike morphology with macroporous structure (Figure 4c,d). The diameter of FE05 was about 7.6 μm, which is smaller than that of the pristine and composite cellulose fibers. The reduced diameter for the fiberlike inorganic materials could be a result of the calcination of the cellulose matrix. When the content of the incorporated Fe_2O_3 nanoparticles in the cellulose fibers is low, the structure for the inorganic materials would collapse,

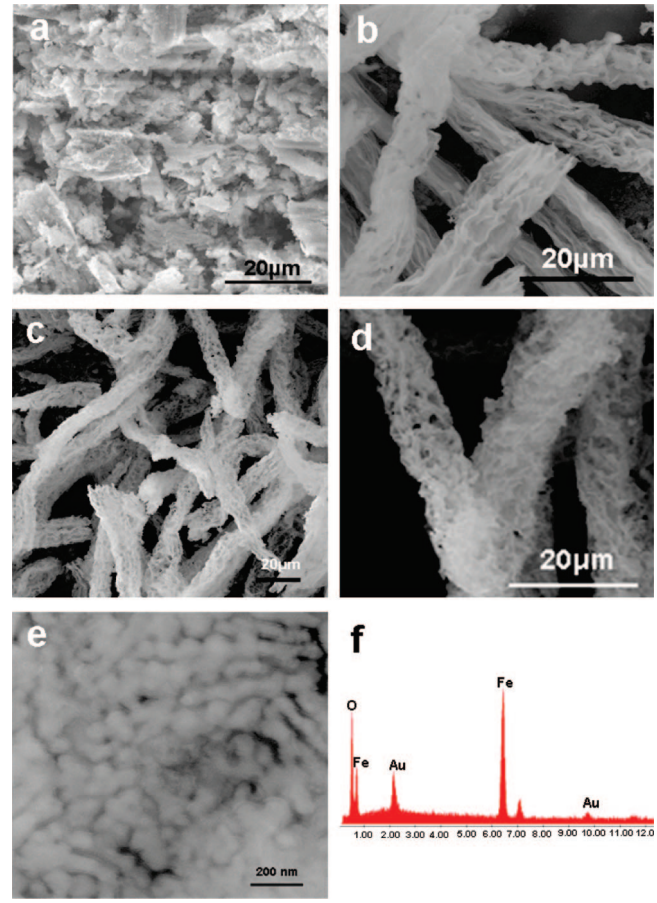

Figure 4. SEM images of the fiberlike Fe_2O_3 macroporous nanomaterials of FE001 (a), FE01 (b), and FE05 (c) and enlarged images (d, e) of FE05 as well as its EDS pattern (f).

as shown in Figure 4a. It is noted that higher content of the incorporated Fe_2O_3 nanoparticles contributes to maintaining the integrated morphology for the inorganic materials because more Fe_2O_3 nanoparticles in the cellulose fibers may form an interconnected network structure and prevent them from collapsing during calcination. The advantage of this method is that the resulting materials possess high porosity as well as large surface area. Figure 4e shows that the fiberlike porous Fe_2O_3 nanomaterials are constituted of individual Fe_2O_3 nanoparticles. The EDS spectrum of FE05 measured from FESEM indicates that there are only O and Fe elements in the inorganic samples (Figure 4f). Therefore, the fiberlike porous Fe_2O_3 nanomaterials have been fabricated successfully by a simple process. This method is easy and cost-effective, and the fiberlike Fe_2O_3 samples could be fabricated on a large scale. The main advantage of this approach is the low amounts of waste, which may be seen as a "green" pathway. As far as we known, it is the first time that fiberlike Fe_2O_3 macroporous nanomaterials are prepared by using regenerated cellulose fibers as templates.

On the basis of the results mentioned above, a schematic illustration for the formation of the fiberlike porous Fe_2O_3 nanomaterials is proposed in Figure 5. When the swollen cellulose fibers were soaked in $FeCl_3$ solution, Fe^{3+}could readily impregnate into the pores of the cellulose fibers. The incorporated Fe^{3+} ions could be bound to the cellulose macromolecules via electrostatic interaction because the electron-rich oxygen atoms of the polar hydroxyl groups of

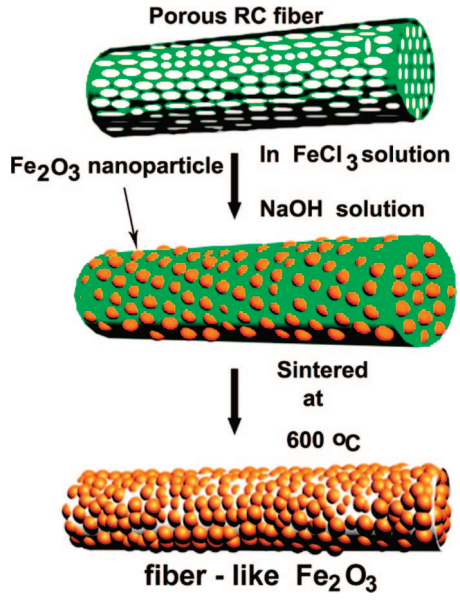

Figure 5. Schematic illustration for the formation of the fiberlike Fe_2O_3 nanomaterials.

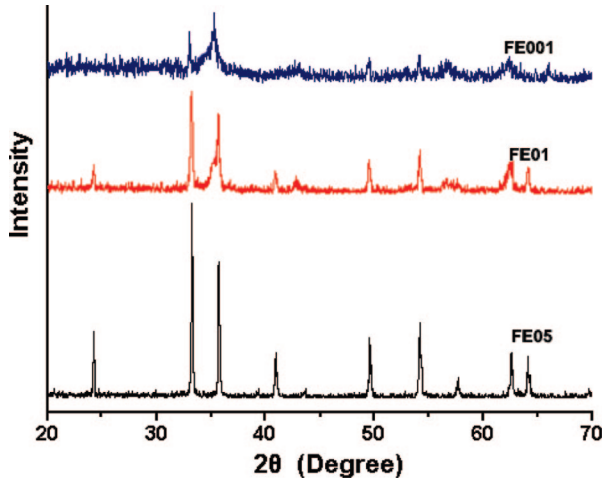

Figure 6. The XRD patterns of the Fe_2O_3 nanomaterials.

cellulose are expected to interact with the electropositive transition metal cations.[36] When the composite fibers were treated with aqueous NaOH solution and rinsed with water, hydrolysis and condensation reactions occurred. Thus, Fe_2O_3 nanoparticles were synthesized in situ in the cellulose fibers to create the Fe_2O_3/cellulose composite fibers. After calcination, the fiberlike Fe_2O_3 could form in the case of high content of Fe_2O_3 nanoparticles in the cellulose fibers. It is clear that the relative high content of Fe_2O_3 nanoparticles in the cellulose fibers is responsible for the formation of the fiberlike Fe_2O_3 because a continuous phase of Fe_2O_3 nanoparticles could be created in the cellulose fibers.

To clarify the phase structure and purity of the synthesized Fe_2O_3 samples, XRD measurements were performed. Figure 6 shows the XRD results for the FE001−FE05 samples. There is no diffraction peak of other impurities except for the Fe_2O_3 component. Compared with standard JCPDS-84-0311 data (Joint Committee on Powder Diffraction Standards), the diffraction patterns are matched with the α-Fe_2O_3 sample perfectly. The results indicate that the porous Fe_2O_3 fibers are composed of high-purity α-Fe_2O_3. Brunauer−Emmett−Teller (BET) nitrogen adsorption−desorption measurements indicate that the specific surface area of the FE001, FE01, and FE05 samples is about 22, 25, and 38 m^2/g, respectively. Considering the factors that affect the specific surface area of materials, it is the pore structure that controles the surface areas and the pore size of the Fe_2O_3 fibers.

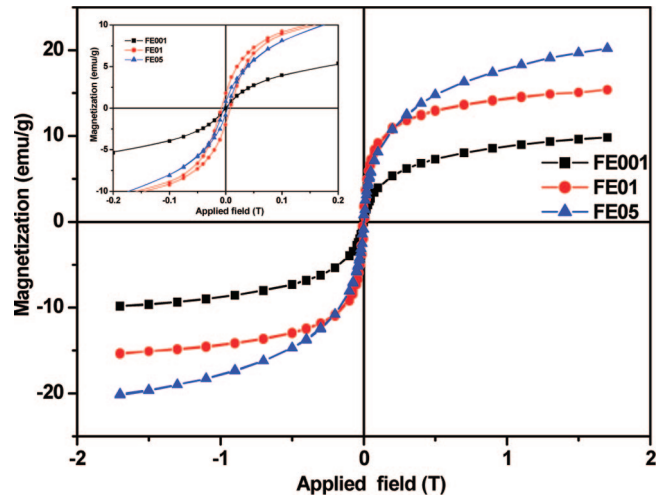

Figure 7. Magnetization of the Fe_2O_3 nanomaterials as a function of the applied magnetic field measured at 298 K.

Figure 7 shows the magnetic properties of the FE001, FE01, and FE05 samples as a function of the applied magnetic field at 298 K. It is clear that the FE001 sample exhibits an extremely small hysteresis loop and coercivity. The absence of hysteresis and coercivity is characteristic of superparamagnetic particles or some single-domain particles.[37,38] It has been known that magnetic particles, which are smaller than some critical particle size, can be called single domains. As the particle size continues to decrease below the single domain value, the particles exhibit superparamagnetic properties. In the case of the FE01 and FE05 samples, both of them exhibite weak ferromagnetic behaviors with small hysteresis loop and coercivity. This result further confirms that the particle size of the prepared Fe_2O_3 samples by this method is small. We believe that the fiberlike magnetic porous nanomaterial is a very promising candidate for various applications, including chemical and biochemical separations.[39]

Figure 8a shows the discharge curves of the Fe_2O_3 electrodes during the first cycle. There are two obvious potential slopes (1.3−1.1 and 1.0−0.9 v) for the reaction of lithium with α-Fe_2O_3, which are similar to those of α-Fe_2O_3 nanoparticles.[40] The dependence of the discharge capacity on the cycle number for the Fe_2O_3 samples is shown in Figure 8b. The first cycles of these electrodes imply an irreversible capacity. It can be attributed to the formation of a solid

(36) Shim, L.-W.; Choi, S.; Noh, W.-T.; Kwon, J.; Cho, J. Y.; Kim, K.-S.; Kang, D. H. *Bull. Korean Chem. Soc.* **2002**, *23*, 563.
(37) Sohn, B. H.; Cohen, R. E. *Chem. Mater.* **1997**, *9*, 264.
(38) Leslie-Pelecky, D. L.; Rieke, R. D. *Chem. Mater.* **1996**, *8*, 1770.
(39) Son, S. J.; Reichel, J.; He, B.; Schuchman, M.; Lee, S. B. *J. Am. Chem. Soc.* **2005**, *127*, 7316.
(40) Larcher, D.; Masquelier, C.; Bonnin, D.; Chabre, Y.; Masson, V.; Leriche, J. B.; Tarascon, J. M. *J. Electrochem. Soc.* **2003**, *150*, A133.

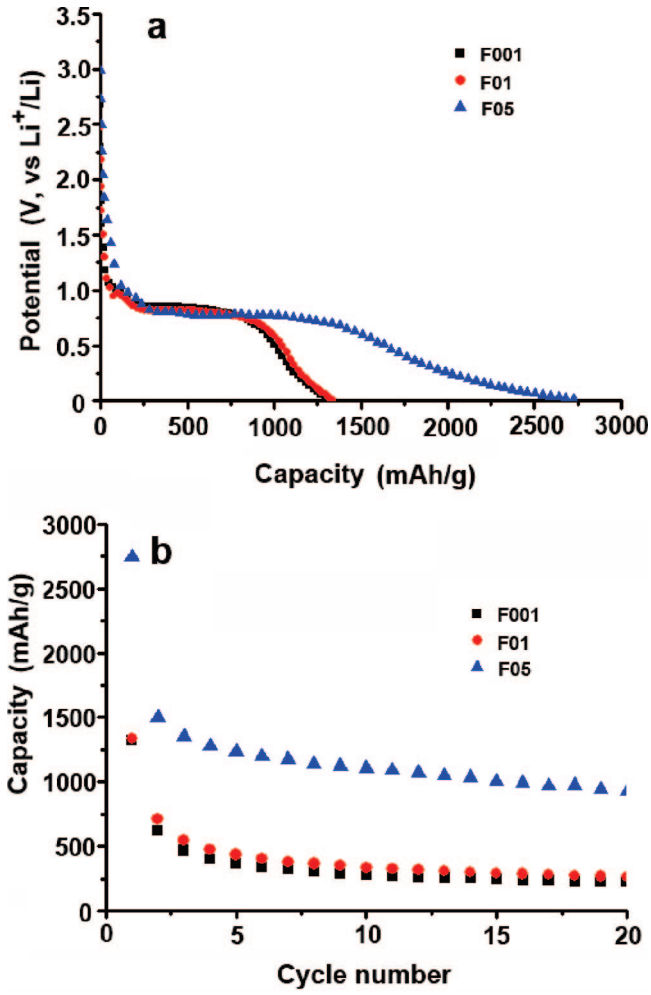

Figure 8. Discharge curves at the first cycles (a) and cycle performance (b) of the electrode made of the α-Fe_2O_3 samples. The discharging current density was 100 mA/g and the working temperature was 20 °C.

electrolyte interface layer on the surface of the electrodes.[41] After the fifth cycle, a stable discharge capacity for each sample has been observed. The discharge capacity of the FE05 sample in the fifth cycles is 1235 mA·h/g, which is much higher than those of FE001 (364 mA·h/g) and FE01 (434 mA·h/g). It has been reported that the three-dimensional nanostructured transition-metal oxides, such as nickel oxides, cobalt oxides, and iron oxides, exhibit reversible capacities about 3 times larger than that of graphite.[42,43] A new mechanism for the formation and decomposition of Li_2O has been proposed as being via the reduction and oxidation of the metal nanoparticles, rather than via insertion/extraction of Li in graphite. Therefore, the superior discharge capacity for the battery made from FE05 sample could be a result of the increased surface area and the porosity of Fe_2O_3 nanomaterials. It is worth noting that the discharge capacity of FE05 in the 10th and 20th cycles was 1102 and 927 mA·h/g, respectively. After 50 cycles, the electrode capacity decreased to 732 mA·h/g, which was about 27% of the initial value. (See Figure S2 in the Supporting Information.) However, this value is still much higher than that of graphite (372 mA·h/g). It suggests that the fiberlike Fe_2O_3 porous nanomaterials possess potentially electro-chemical properties that can serve as alternative anode materials for Li-ion batteries.

(41) Frackowiak, E.; Gautier, S.; Gaucher, H.; Bonnamy, S.; Beguin, F. *Carbon* **1999**, *37*, 61.
(42) Poizot, P.; Laruelle, S.; Grugeon, S.; Dupont, L.; Tarascon, J. M. *Nature* **2000**, *407*, 496.
(43) Larcher, D.; Bonnin, D.; Cortes, R.; Rivals, I.; Personnaz, L.; Tarascon, J. M. *J. Electrochem. Soc.* **2003**, *150*, A1643.

Conclusions

The cellulose/Fe_2O_3 composite fibers were easily fabricated in situ by first incorporating a large amount of Fe^{3+} into the macroporous structures of the swollen regenerated cellulose fibers, followed by treatment with NaOH solution. After calcination of the composite fibers, the fiberlike Fe_2O_3 macroporous nanomaterials were obtained. The concentration of $FeCl_3$ solution plays an important role in controlling the Fe_2O_3 content in the composite cellulose fibers and the morphologies of the resulting Fe_2O_3 nanomaterials. The 1D macroporous nanomaterials with high pure α-Fe_2O_3 possessed high BET surface area and weak ferromagnetic properties. Moreover, they exhibited novel electrochemical activity and could be used as alternative anode materials for lithium-ion battery. The advantages of this method are its simplicity, cost-effectiveness, and scalable production of the 1D fiberlike Fe_2O_3 nanomaterials. This work provides a new conceptual scheme for the design and fabrication of 1D inorganic nanomaterials.

Acknowledgment. This work was supported by the National Support Project for Science and Technology (2006BAF02A09), a major grant of the National Natural Science Foundation of China (59933070 and 30530850), and the National Natural Science Foundation of China (20474048 and 20674057).

Note Added after ASAP Publication. There was an error in Figure 8 in the version published ASAP May 10, 2008; the corrected version was published ASAP May 16, 2008.

Supporting Information Available: SEM images and discharge curves of the electrode (pdf). This material is available free of charge via the Internet at http://pubs.acs.org.

CM703623V